Received: 8 July 2020 | Revised: 21 August 2020 | Accepted: 24 August 2020

DOI: 10.1002/jcp.30039

ORIGINAL RESEARCH ARTICLE

Journal of Cellular Physiology WILEY

# Involvement of oxidative stress-induced annulus fibrosus cell and nucleus pulposus cell ferroptosis in intervertebral disc degeneration pathogenesis

Run-Ze Yang | Wen-Ning Xu | Huo-Liang Zheng | Xin-Feng Zheng | Bo Li | Lei-Sheng Jiang | Sheng-Dan Jiang

Department of Clinic of Spine Center, Xinhua Hospital, School of Medicine, Shanghai Jiao Tong University, Shanghai, China

**Correspondence**
Lei-Sheng Jiang and Sheng-Dan Jiang, Department of Clinic of Spine Center, Xinhua Hospital, School of Medicine, Shanghai Jiao Tong University, No. 1665, Kongjiang Rd, Yangpu, Shanghai 200092, China.
Email: jiangleisheng@xinhuamed.com.cn (L.-S. J.) and jiangshengdan@xinhuamed.com.cn (S.-D. J.)

**Funding information**
National Natural Science Foundation of China, Grant/Award Number: 81672206

## Abstract

Ferroptosis is a necrotic form of regulated cell death that was associated with lipid peroxidation and free iron-mediated Fenton reactions. It has been reported that iron deficiency had been implicated in the pathogenesis of intervertebral disc degeneration (IVDD) by activating apoptosis. However, the role of ferroptosis in the process of IVDD has not been illuminated. Here, we demonstrate the involvement of ferroptosis in IVDD pathogenesis. Our in vitro models show the changes in protein levels of ferroptosis marker and enhanced lipid peroxidation level during oxidative stress. Safranin O staining, hematoxylin-eosin staining, and immunohistochemical were used to assess the IVDD after 8 weeks of surgical procedure in vivo. Treatment with ferrostatin-1, deferoxamine, and RSL3 demonstrate the role of ferroptosis in *tert*-butyl hydroperoxide (TBHP)-treated annulus fibrosus cells (AFCs) and nucleus pulposus cells (NPCs). Ferritinophagy, nuclear receptor coactivator 4 (NCOA4)-mediated ferritin selective autophagy, is originated during the process of ferroptosis in response to TBHP treatment. Knockdown and overexpression NCOA4 further prove TBHP may induce ferroptosis of AFCs and NPCs in an autophagy-dependent way. These findings support a role for oxidative stress-induced ferroptosis in the pathogenesis of IVDD.

**KEYWORDS**
Ferroptosis, intervertebral disc degeneration, NCOA4, oxidative stress

## 1 | INTRODUCTION

Regulated cell death (RCD), such as apoptosis, plays an important role in a variety of physiological processes, including organogenesis and maintaining homeostasis. Abnormal regulation of RCD is involved in the onset and development of many human diseases (Pasparakis & Vandenabeele, 2015). Ferroptosis, a recently recognized type of RCD, has been identified as an iron-dependent and caspase-independent nonapoptotic cell death. Among RCDs, ferroptosis is identified as an iron-dependent RCD, which characterized by lipid peroxidation of cell membrane attributed to reactive oxygen species (ROS) generated in the iron-mediated Fenton reaction (Dixon et al., 2012; Stockwell et al., 2017). Ferroptosis is different from other typical nonapoptotic cell death via its morphological features of mitochondrial shrinkage and increased density

Run-Ze Yang and Wen-Ning Xu contributed equally to this work.

of mitochondrial membrane, biochemical features of accumulated iron and lipid ROS, and genetic features of involvement of a distinctive set of genes (Angeli, Shah, Pratt, & Conrad, 2017; Xie et al., 2016). Glutathione peroxidase 4 (GPx4), the lipid repair enzyme and a member of the selenoprotein family, has been illustrated to repress the activity of ferroptosis by reducing lipid hydroperoxidation (Friedmann Angeli et al., 2014; Imai et al., 2003).

Ferroptosis has been involved in some pathophysiological environments, such as degenerative diseases, tumorigenesis, and stroke (Angeli et al., 2017; Xie et al., 2016). It has been reported recently that inactivation of Gpx4 in mice caused ferroptosis in kidney tubular cells, inducing acute renal failure, which was efficiently prevented by a specific ferroptosis inhibitor ferrostatin-1 (Fer-1; Friedmann Angeli et al., 2014), and that deferoxamine, compound 968, and Fer-1, all of which inhibit glutaminolysis and ferroptosis, limit myocardial I/R injury ex vivo (Gao, Monian, Quadri, Ramasamy, & Jiang, 2015). Although the ferroptosis has been found involved in disease pathogenesis such as renal and brain injury models (Friedmann Angeli et al., 2014; Li et al., 2017; Linkermann, Stockwell, Krautwald, & Anders, 2014; Martin-Sanchez et al., 2017), the participation of ferroptosis in the spinal diseases, including intervertebral disc degeneration (IVDD), remains unclear.

Low back pain (LBP) is a common symptom in middle-aged and elderly people. There are many factors that can cause chronic LBP, such as aging, genetics, and lifestyle, severely lowering the life quality of human beings (Jensen, Riis, Petersen, Jensen, & Pedersen, 2017). IVDD is widely acknowledged to be a leading cause of LBP (Cao et al., 2015; Yang et al., 2015, 2016), causing huge social and economic burdens. intervertebral discs (IVDs) are fibrocartilage tissues located between the vertebrae; these tissues function as shock absorbers by distributing mechanical loads along the spine and promoting flexibility in the trunk (Henry, Clouet, Le Bideau, Le Visage, & Guicheux, 2018). A normal IVD consists of an external fibrous ring (AF), which forms an annular structure to surround the nucleus pulposus (NP) and is connected to the adjacent vertebral body through a cartilage endplate (Le Maitre, Binch, Thorpe, & Hughes, 2015). AF and NP have an essential role in maintaining the normal function of IVD. Multiple reasons, such as oxidative stress, trauma, infection, inflammation, are involved in the occurrence and development of IVDD (Feng et al., 2016; Vo et al., 2013).

In the process of IVDD, degeneration of the cartilage endplates, annulus fibrosus rupture, and inflammation, exacerbate oxidative stress in nucleus pulposus cells (NPCs) through inducing ROS production (Shamji et al., 2010). In the initiation and progression of IVDD, aggressive oxidative stress, inducing mitochondrial apoptosis in NPCs (Nasto et al., 2013; Nerlich et al., 2007), accelerating cell aging (Dimozi, Mavrogonatou, Sklirou, & Kletsas, 2015; Jeong, Lee, & Kim, 2014) and inducing autophagy in annulus fibrosus cells (AFCs; W. N. Xu et al., 2019), has an essential role. It has been reported that ROS, oxidative stress, and autophagy also participates in the process of ferroptosis (Lee et al., 2020). A recent study has discovered that labile iron is produced by autophagic ferritin degradation in a process termed ferritinophagy (Mancias, Wang, Gygi, Harper, & Kimmelman, 2014). This new form of autophagy lies in the selective ferritin receptor nuclear receptor coactivator 4 (NCOA4), which transports ferritin to the autophagosome (Dowdle et al., 2014). More importantly, according to the latest news, ferritinophagy can promote the process of ferroptosis (Gao et al., 2016; Hou et al., 2016). Therefore, we hypothesized that oxidative stress may induce ferroptosis of AFCs and NPCs in an autophagy-dependent way.

## 2 | MATERIALS AND METHODS

### 2.1 | Cell culture and patient specimens obtain

According to the previous research method (X. Wang et al., 2014), SD rat AF cells and NP cells were acquired. AF cells and NP cells were cultured in DMEM/F12 modified medium (Gibco, Invitrogen). All medium contained 10% fetal bovine serum, 100 units/ml penicillin, and 100 μg/ml streptomycin. Cells were cultured in a humidified atmosphere of 5% CO2 at 37°C. To investigate whether ferroptosis could occur in AF and NP cells in the event of oxidative stress, cells were exposed to *tert*-butyl hydroperoxide (TBHP) for different concentrations (0, 50, 100, 200 μM) to determine the best concentration. Human disc tissues were obtained from patients who had undergone elective spinal surgery. Human disc tissue collection and experiments were approved by the Ethics Committee of Xinhua Hospital Affiliated with the Shanghai Jiao Tong University School of Medicine. All experiments involving human specimens followed the Helsinki declaration (World Medical Association, 2014).

### 2.2 | Reagents and antibodies

The following reagents were used: Fer-1 (HY-100579; MedChemExpress), deferoxamine mesylate (DFO; HY-B0988; MedChemExpress), RSL3 (HY-100218A; MedChemExpress), 3-methyladenine (3-MA; M9281; Sigma-Aldrich).

The antibodies used were mouse anti-FTH (sc-376594; Santa Cruz), mouse anti-GPX4 (sc-166570; Santa Cruz), rabbit anti-PTGS2 (12375-1-AP; ProteinTech), mouse anti-ACSL4 (sc-365230; Santa Cruz), rabbit anti-NCOA4 (PA5-36391; Thermo Fischer Scientific), rabbit anti-LC3 (NB600-1384; Novus), rabbit anti-P62 (18420-1-AP; ProteinTech), mouse anti-GAPDH (60004-1-Ig; ProteinTech), rabbit anti-ferritin (ab75973; Abcam).

### 2.3 | Quantitative reverse transcription-polymerase chain reaction analysis

For detecting messenger RNA, the tissue were lysed and TRIzol reagent (Invitrogen) was used to extract the total RNA. Complementary DNA templates were generated by using the PrimeScript™ RT reagent Kit with gDNA Eraser (Takara). Reverse transcription-polymerase chain reaction (RT-PCR) was carried out on the Mx3000P system (Stratagene) by using the SYBR Premix Ex Taq™ II Kit (Takara) according to the instruction. As for microRNA (miRNA) detection, the miRNAs were isolated using miRNA Isolation Kit (BioFlux). RT-PCR was

proceeded using All-in-One™ miRNA Fist-Strand cDNA Synthesis Kit (GeneCopoeia) and All-in-One™ miRNA qPCR Kit (GeneCopoeia) with RNU6-2 as the internal reference. The $2^{-\Delta\Delta C_t}$ method was used to estimate the relative expression level of the miRNAs.

## 2.4 | Western blotting

Western blotting was conducted as previously described (Fujii et al., 2012). Briefly, the proteins were harvested from cell lysates using radioimmunoprecipitation assay (Beyotime) including phenylmethylsulfonyl fluoride (Beyotime) after AF and NP cells were washed by ice-cold phosphate-buffered saline (PBS). Protein concentrations were detected by the BCA Protein Assay Kit (Beyotime). Equal amounts of total protein were resolved by 8%–12% sodium dodecyl sulfate–polyacrylamide gel electrophoresis in each experiment and transferred to polyvinylidene difluoride membrane (Millipore). Then the membranes were blocked in Blocking Buffer (Beyotime) and were incubated with a specific primary antibody at 4°C overnight. After that membranes were washed with TBST three times and incubated with horseradish peroxidase (HRP)-conjugated secondary antibodies. Finally, using chemiluminescence detection (34080; Thermo Fisher Scientific and 1705061; Bio-Rad) with the ChemiDocTM Touch Imaging System (Bio-Rad) to get results. The results were quantified by ImageJ (National Institutes of Health).

## 2.5 | Lactate dehydrogenase release assay

IVD cell death was detected by the lactate dehydrogenase (LDH) release assay, which can reflect the integrity of the cell membrane, using the LDH Cytotoxicity Assay Kit (Beyotime). AFCs and NPCs were transferred into 96-well plates and then 100 μl of LDH reaction solution was added to each well for 30 min. Finally, using a Microplate Reader (Bio-Rad) to detect the absorbance at 490 nm.

## 2.6 | Lipid peroxidation assay

A lipid peroxidation sensor, BODIPY™ 581/591 C11 (D3861; Thermo Fisher Scientific), was used to measure the lipid peroxidation level in vitro according to the manufacturer's instruction. Briefly, cells were incubated for 30 min with BODIPY 581/591 C11 (2 μM) in a serum-free medium. Images were acquired under fluorescence microscopy (BX51; Olympus). Fluorescence of the sensor was monitored by simultaneous acquisition of the green (484/510 nm) and red signals (581/610 nm), providing a ratio index of lipid peroxidation.

## 2.7 | Transmission electron microscopy

Electron microscopy was performed to monitor the occurrence of autophagy and morphological changes in the cell interior according to the previous study (Cao et al., 2017). After being treated with 100 μM TBHP or 100 μM TBHP and 10 μM Fer-1 for 3 h, AF and NP cells were dissociated and fixed in 2.5% ice-cold glutaraldehyde overnight and postfixed in osmium tetroxide. After that, before being rinsed with propylene oxide and impregnated with epoxy resin, the cells were dehydrated with a series of alcohol concentrations. Uranyl acetate and lead citrate were used by microscopy as a negative control. Electron micrographs were obtained by transmission electron microscope (TEM) according to the means reported by Wang et al. (2013).

## 2.8 | Immunofluorescence examination

Immunofluorescence staining was performed as formerly depicted (Ito et al., 2015). After removing medium and washing with PBS, treated AF and NP cells were then fixed with 4% paraformaldehyde for 15 min followed by permeabilization with 0.03% Triton X-100 (Beyotime) for 60 min and blocked with 5% BSA (Beyotime) for 60 min. After that, cells were incubated with the primary antibodies at 4°C overnight in a humidified box. On the following morning, cells were washed and incubated with fluorescein isothiocyanate- or tetramethylrhodamine isothiocyanate-conjugated second antibodies for 1 h and labeled with DAPI (Beyotime) for 5 min. The fluorescence intensity of GPX4 and ferritin heavy chain (FTH) were analyzed by the fluorescence microscopy (Olympus BX51).

## 2.9 | Monitoring autophagic flux by tandem mRFP-GFP-LC3

To detect the autophagic flux, cells were transfected with mRFP-GFP-LC3 adenovirus (Hanbio Co. Ltd.). AF and NP cells were transfected with tandem fluorescent mRFP-GFP-tagged adenovirus for 48 h following the manufacturer's instruction and then fluorescence microscopy (Olympus BX51) was used to monitor LC3 puncta after other treatments.

## 2.10 | Co-immunoprecipitation assay

Cells were collected by centrifugation at 300*g* for 10 min and lysed with ice-cold cell lysis buffer (Beyotime Biotechnology). A specific protein antibody against the target protein was incubated with Protein G Agarose beads (Invitrogen) for 3 h at 4°C, and the lysate was then added to the mixture. The mixture was incubated at 4°C overnight. After that, the mixture was washed three times with ice-cold PBS, the co-immunoprecipitation (Co-IP) product was harvested, and western blotting was used to analyze the proteins.

## 2.11 | Small interfering RNA transfection

NCOA4 si-RNA was purchased from the manufacturer (Genomeditech). The consequence was listed as follow: si-NCOA4-1 (sense:

5′-GCCCUACAAUGUGAAUGAU-3′ and antisense: 5′-AUCAUUC-ACAUUGUAGGGC-3′), si-NCOA4-2 (sense: 5′-GGCCAAUUCAAU UGUCUUA-3′ and antisense: 5′-UAAGACAAUUGAAUUGGCC-3′), and si-NCOA4-3 (sense: 5′-GCUCAUCCUAGUUCUUCAA-3′ and antisense: UUGAAGAACUAGGAUGAGC-3′). Small interfering RNA (si-RNA) was transfected into AF and NP cells by using Lipofectamine 3000 reagent (Invitrogen). si-NC was used as a negative control.

### 2.12 | Lentivirus transfection

Lenti-NCOA4 or lenti-NC was added into the medium at 60%–80% cell density. The medium was then removed and replaced with a fresh medium. Western blotting and fluorescence microscope were used to detect the transfection efficiency.

### 2.13 | Surgical procedure

Rat experiments were conducted according to the International Guiding Principles for Biomedical Research Involving Animals and were approved by our University Ethics Committee (Ethics Committee of Xinhua Hospital Affiliated with Shanghai Jiao Tong University School of Medicine). A total of 15, 10-week-old male Sprague-Dawley (SD) rats were randomly divided into three groups (control group, saline group, and deferoxamine group), then proceeded intraperitoneal injection with 2% (wt/vol) pentobarbital according to the weight (40 mg/kg). Perform model surgery on the saline group and deferoxamine group. As mentioned before (Han et al., 2008), the operation section of rat tail disc (Co7/8) was located by palpation on the coccygeal vertebrae and confirmed by the X-ray radiograph. Needles (20-G) were used to puncture the AF through the tail skin perpendicularly and all the needles were revolved 360°. After the operation, the deferoxamine solution (50 mg/ml) was immediately injected intraperitoneally 0.2 mg/g/day until the rat was killed. The saline group was given the same amount of normal saline. The rats are monitored daily to ensure their health, and all rats are allowed to carry and exercise freely and without restrictions.

### 2.14 | Magnetic resonance imaging method

After 8 weeks of model operation, the animals were performed the magnetic resonance imaging (MRI) examination.

### 2.15 | Histopathologic analysis

The rats were killed by an intraperitoneal overdosage injection of 10% pentobarbital and the tails were obtained on 8 weeks after surgery. Specimens were fixed with formaldehyde and then decalcified, after that dehydrated and embedded in paraffin. The tissues were cut into 5-mm sections. The disc specimens were stained with safranin O-fast green (S-O) and hematoxylin-eosin (HE) staining. The structure of discs was observed by a microscope.

### 2.16 | Immunohistochemical examination

The sections were deparaffinized and rehydrated and then antigen was retrieved in microwaved for 15 min each. Then, endogenous peroxidase activity was blocked for 10 min by 3% hydrogen peroxide, and nonspecific binding sites were blocked for 30 min at room temperature by 5% BSA. The primary antibodies (GPX4, FHT, LC3) were added to sections and incubated overnight at 4°C. The sections were incubated with an appropriate HRP-conjugated secondary antibody and counterstained with hematoxylin.

### 2.17 | Statistical analysis

All the experiments were performed at least three times. The results were expressed as mean ± *SD*. Statistical analyses were performed using the SPSS statistical software program 20.0. In addition, the Student's *t*-test was used to analyze the significant differences between the two independent groups, and the differences between the multiple groups were compared by one-way analysis of variance. $^{*}p < .5$, $^{**}p < .01$, $^{***}p < .001$ represents the difference.

## 3 | RESULTS

### 3.1 | Compared with normal IVD tissue, ferroptosis occurred in degenerated IVD tissue

To investigate whether degenerative disc tissue occurs ferroptosis, patients with hemivertebral disc tissue were collected as the normal group and those with lumbar disc herniation as the degenerative group. Quantitative RT-PCR results showed that the GPX4 level of the degenerative group was downregulated and the prostaglandin-endoperoxide synthase 2 (PTGS2) level was upregulated in the contrast of normal group (Figure 1a,b). It is obviously found that the expression of GPX4 and FTH was decreased and PTGS2 was increased in the degenerative group compared with the normal group (Figure 1c). The ratio of GPX4/β-actin, FTH/β-actin, and PTGS2/β-actin further implied that ferroptosis occurred in the degenerative disc tissue (Figure 1d–f).

### 3.2 | Oxidative stress-induced ferroptosis in rat AFCs and NPCs

To simulate the role of oxidative stress during IVDD, AFCs and NPCs were exposed to TBHP at a different concentration (50, 100, and 200 μM) for 3 h. LDH assay demonstrated that the cell death rate of AFCs and NPCs increased with growing TBHP concentration

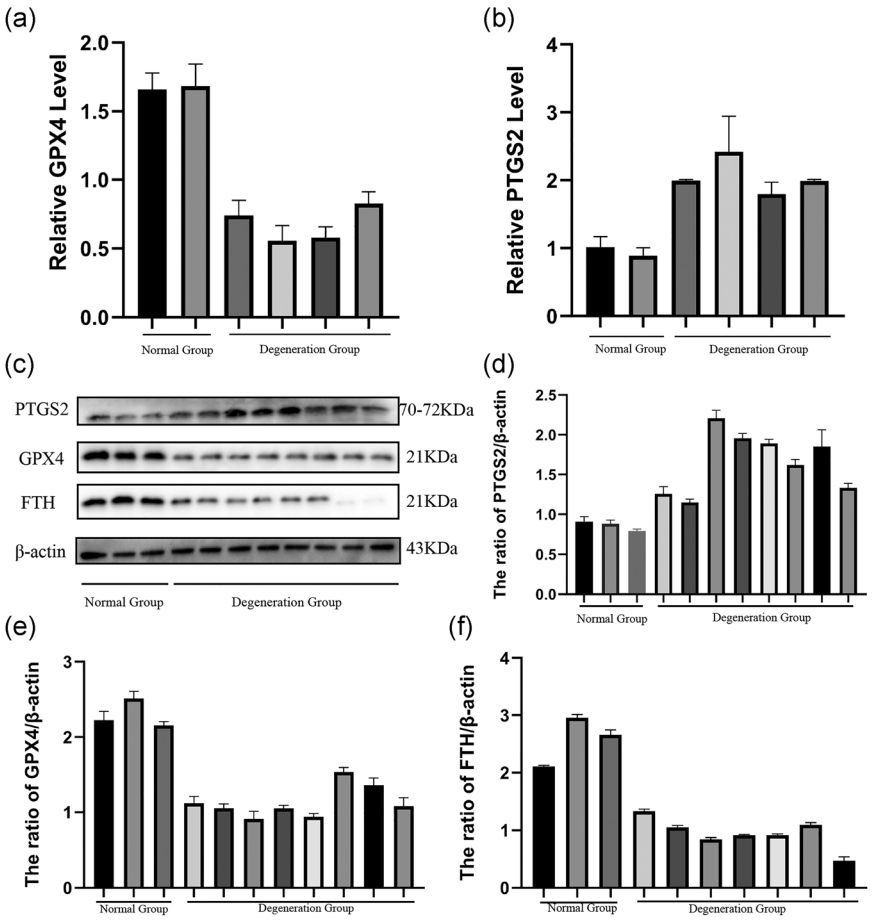


**FIGURE 1** Ferroptosis was involved in the process of intervertebral disc degeneration. We collected normal disc tissue and degenerated disc tissue for comparison. Patients' information was collected and summarized in the supplementary file. (a, b) The difference in messenger RNA expression of ferroptosis markers glutathione peroxidase 4 (GPX4) and prostaglandin-endoperoxide synthase 2 (PTGS2) in normal and degenerated intervertebral disc tissues. (c) Protein expression of PTGS2, GPX4, ferritin heavy chain (FTH), and β-actin in normal group and degeneration group. (d–f) The relative ratio of protein (PTGS2, GPX4, FTH) to β-actin

(Figure S1a,b). Western blotting showed that the expression of FTH and GPX4 was decreased and the expression of PTGS2 and long-chain acyl-CoA synthetase 4 (ACSL4) were increased with the increase of TBHP concentration (Figures 2a and 2e). Figures 2b and 2f also confirmed that TBHP induced the expression of ferroptosis marker proteins to change in AFCs and NPCs. Lipid peroxidation assay suggested that the lipid peroxidation level of AFCs and NPCs increased, as the concentration of TBHP increased (Figures 2c and 2g). The main morphological characteristics of ferroptosis under TEM performed those dense and smaller mitochondria with increased membrane density and vestigial cristae (Dixon et al., 2012). To confirm these morphological features, TEM evaluation was carried on in TBHP-exposed AFCs and NPCs. Dense and shrunken mitochondria were highly obvious in TBHP treated AFCs and NPCs compared with the NC group cells (Figures 2d and 2h).

## 3.3 | Cell death in AFCs and NPCs caused by TBHP could be specifically suppressed and was similar to ferroptosis caused by RSL3

To further determine whether oxidative stress-induced disc degeneration occurred ferroptosis, we used DFO, Fer-1, ferroptosis specific inhibitors, and RSL3, ferroptosis specific inducer. Western blotting results indicated that ferroptosis specific inhibitors, DFO and Fer-1, could reverse the downtrend of the expression of FTH and GPX4, and ferroptosis specific inducer, RSL3, could also cause the gradual downtrend of the expression of FTH and GPX4 with the RSL3 consistence increased (Figures 3a and 3f). Figures 3b,c and 3g,h also suggested TBHP induced cell death in AFCs and NPCs was similar to RSL3 induced and was suppressed by DFO and Fer-1. We can easily find out that DFO weakens the high level of lipid peroxidation in AFCs and NPCs treated TBHP and RSL3 also induced uptrend of the lipid peroxidation in AFCs and NPCs by Figures 3d and 3i. Immunofluorescence experiment illustrated that AFCs and NPCs exposed to TBHP and Fer-1 had higher fluorescence intensity of FTH compared with the cells which only treated TBHP and the fluorescence intensity of FTH of AFCs and NPCs exposed to RSL3 were lower (Figures 3e and 3j). The results of the LDH release assay showed that the ratio of cell death in TBHP induced AFCs and NPCs was decreased when using DFO or Fer-1 to inhibit ferroptosis; however, the ratio of cell death was gradually upregulated with the increased concentration of RSL3 (Figure S1c–f).

## 3.4 | Ferritinophagy was involved in TBHP-induced cell death

It has been shown that autophagic degradation of ferritin accumulates labile iron and promotes ferroptosis (Gao et al., 2016;

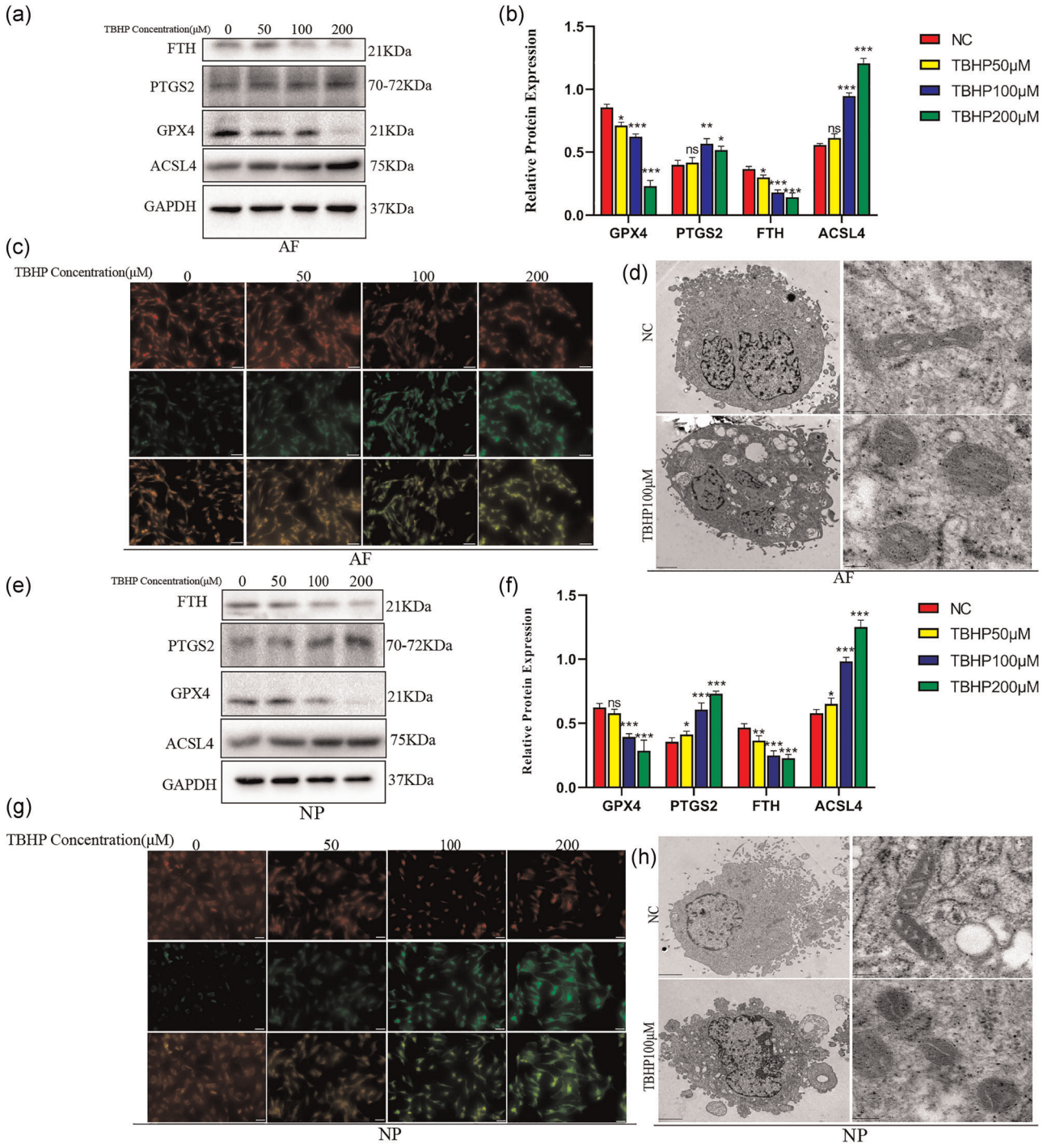


**FIGURE 2** *tert*-Butyl hydroperoxide (TBHP) treatment induced ferroptosis occurred in annulus fibrosus cells (AFCs) and nucleus pulposus cells (NPCs). AFCs and NPCs were exposed to TBHP at different concentration (0, 50, 100, and 200 μM). (a) Protein expression of ferritin heavy chain (FTH), prostaglandin-endoperoxide synthase 2 (PTGS2), glutathione peroxidase 4 (GPX4), acyl-CoA synthetase 4 (ACSL4), and GAPDH in AFCs treated TBHP. (b) The difference in GPX4, PTGS2, ACSL4, and FTH expression in AFCs stimulated by different TBHP concentrations. (c) Lipid peroxidation level of AFCs after treatment with different concentrations of TBHP. (d) Observation of AFCs morphologic change after treatment with TBHP by a transmission electron microscope (TEM). (e) Protein expression of FTH, PTGS2, GPX4, ACSL4, and GAPDH in NPCs treated TBHP. (f) The difference in GPX4, PTGS2, ACSL4, and FTH expression in NPCs stimulated by different TBHP concentrations. (g) Lipid peroxidation level of NPCs after treatment with different concentrations of TBHP. (h) Observation of NPCs morphologic change after treatment with TBHP by a TEM. ***$p < .001$, **$p < .01$, *$p < .05$ ($n = 3$)

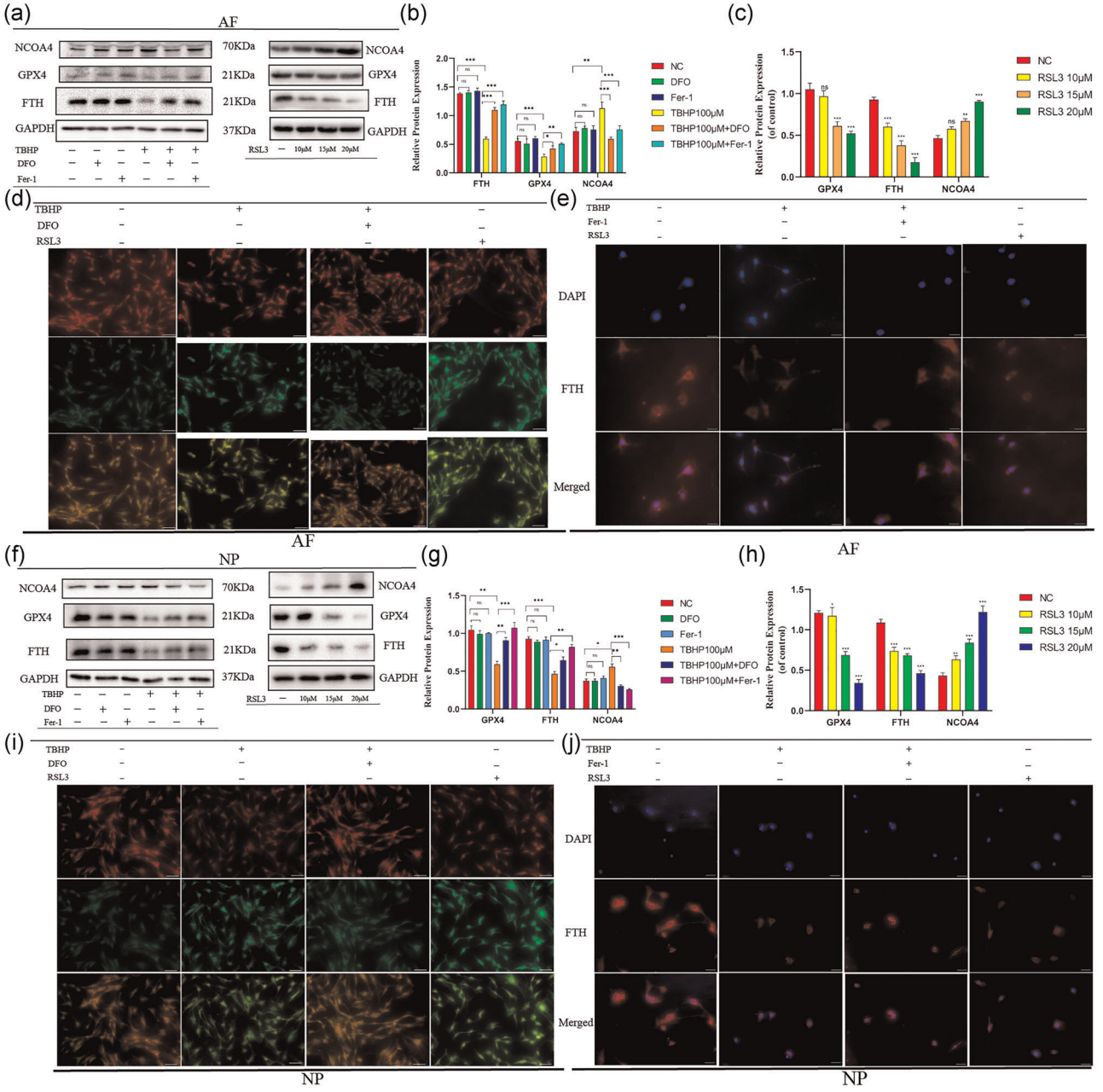


**FIGURE 3** Cell death of annulus fibrosus cells (AFCs) and nucleus pulposus cells (NPCs) induced by *tert*-butyl hydroperoxide (TBHP) was inhibited and was similar to RSL3-induced AFCs and NPCs ferroptosis. AFCs and NPCs were treated with 100 μM TBHP with or without the specific inhibitors deferoxamine mesylate (DFO; 10 μM) or ferrostatin-1 (Fer-1; 5 μM) or were exposed to RSL3 at different concentration (0, 10, 15, 20 μM). (a) Western blotting assay of nuclear receptor coactivator 4 (NCOA4), glutathione peroxidase 4 (GPX4), ferritin heavy chain (FTH), and GAPDH in AFCs. (b,c) The difference in GPX4, NCOA4, and FTH expression in AFCs under different treatments. (d) Lipid peroxidation level under different treatment conditions of AFCs. (e) Immunofluorescence detection of FTH in AFCs. (f) Western blotting assay of NCOA4, GPX4, FTH, and GAPDH in NPCs. (g,h) The difference in GPX4, NCOA4, and FTH expression in NPCs under different treatments. (i) Lipid peroxidation level under different treatment conditions of NPCs. (j) Immunofluorescence detection of FTH in NPCs. $^{***}p < .001$, $^{**}p < .01$, $^{*}p < .05$ ($n = 3$)

Hou et al., 2016). In agreement with this observation, P62, an autophagy marker protein, declined and LC3II, another autophagy marker protein, increased with the increase of TBHP concentration (Figures 4a and 4c). The ratio of LC3II/LC3I in AFCs and NPCs was upregulated with the growing TBHP concentration (Figures 4b and 4d). Figure S2a,b further demonstrated the change of expression level of autophagy-related proteins. It suggested that the autophagy level was upregulated in AFCs and NPCs exposed to TBHP. We also used RSL3 to induce ferroptosis of AFCs and NPCs to monitor changes in autophagy-related proteins. The results suggested that the level of autophagy was also increased in AFCs and NPCs exposed to RSL3 (Figure S1g–k). The expression of NCOA4, a

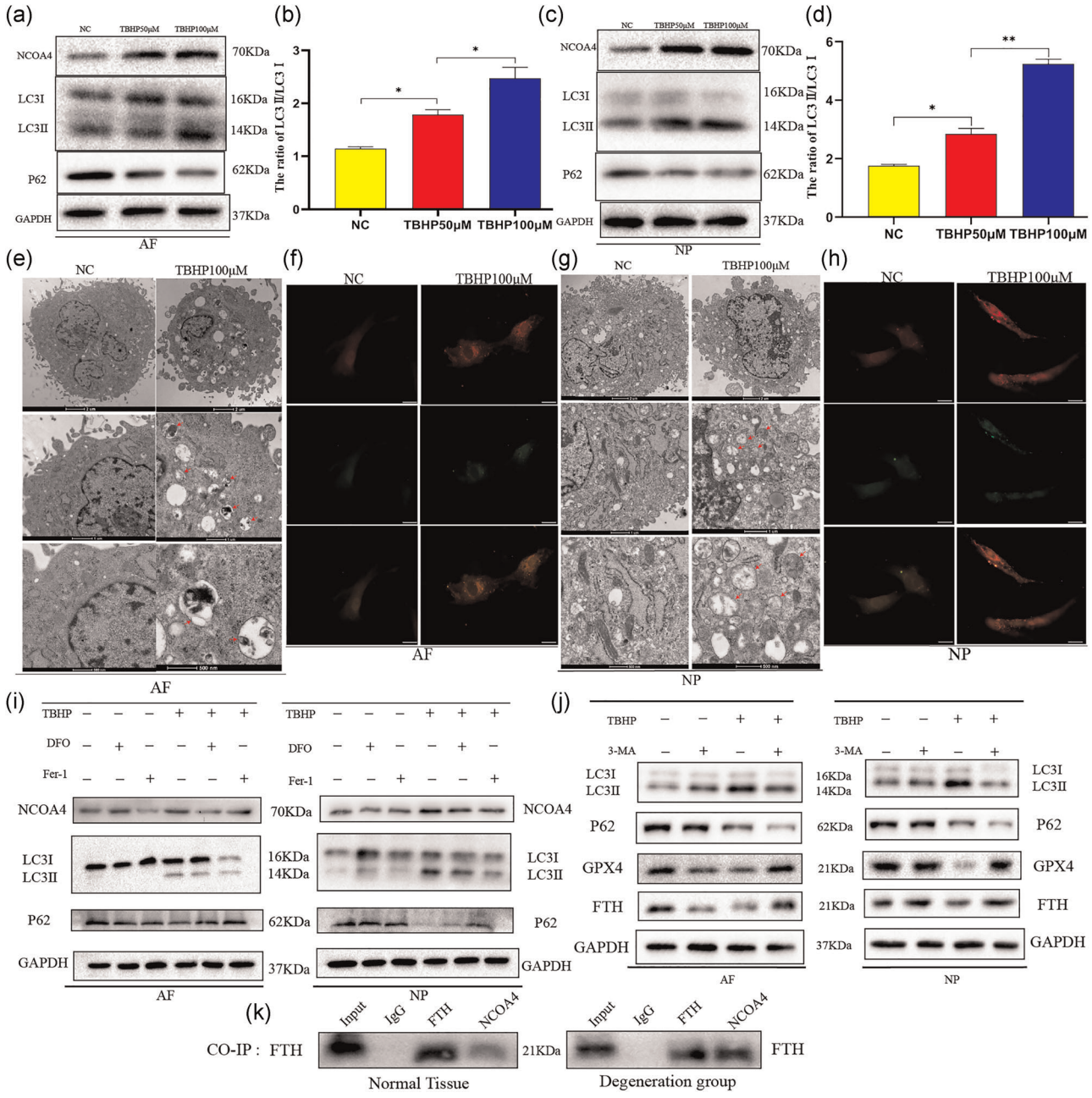


**FIGURE 4** *tert*-Butyl hydroperoxide (TBHP)-induced ferroptosis of annulus fibrosus cells (AFCs) and nucleus pulposus cells (NPCs) in an autophagy-dependent manner. (a) Protein expression of nuclear receptor coactivator 4 (NCOA4), LC3, P62, and GAPDH in AFCs exposed to TBHP. (b) The ratio of LC3II/LC3I in AFCs under different concentrations of TBHP. (c) Protein expression of NCOA4, LC3, P62, and GAPDH in NPCs exposed to TBHP. (d) The ratio of LC3II/LC3I in NPCs under different concentrations of TBHP. (e) Transmission electron microscopy showed increased autophagosomes of AFCs after TBHP stimulation. (f) Fluorescence images of AFCs transfected with mRFP-GFP-LC3 adenovirus. The promotion of Red dot represents that the autophagy was enhanced. (g) Transmission electron microscopy showed increased autophagosomes of NPCs after TBHP stimulation. (h) Fluorescence images of NPCs infected with mRFP-GFP-LC3 adenovirus showed the level of autophagy promoted after TBHP treatment. (i) AFCs and NPCs were exposed to 100 μM TBHP with or without deferoxamine mesylate (DFO; 10 μM) or ferrostatin-1 (Fer-1; 5 μM) for 3 h. The cell lysates were analyzed for the expression of NCOA4, LC3, P62, GAPDH by western blotting. (j) AFCs and NPCs were treated with TBHP (100 μM) with or without 3-methyladenine (3-MA; 10 μM). Western blotting assay of LC3, P62, glutathione peroxidase 4 (GPX4), ferritin heavy chain (FTH), and GAPDH in AFCs and NPCs. (k) Co-immunoprecipitation (Co-IP) test analyzed the relationship between FTH and NCOA4

protein-mediated ferritinophagy, was also upregulated (Figures 4a and 4c). TEM results illustrated that increased autophagosomes in AFCs and NPCs after TBHP treatment compared with normal cells (Figures 4e and 4g). Fluorescence images of AFCs and NPCs infected with mRFP-GFP-LC3 adenovirus showed that red dot increased after TBHP treatment and it also demonstrated increased autophagy (Figures 4f and 4h). The upward level of autophagy and ferritinophagy in AFCs and NPCs could be reversed, when we used specific ferroptosis inhibitors, DFO and Fer-1 (Figures 4i and S2c,d). Western blotting results indicated that the expression of GPX4 and FTH were increased when we used 3-MA to inhibit autophagy in the contrast of cells only treated TBHP (Figures 4j and S2e,f). From the CO-IP test, it is obvious that NCOA4 can be coupled with FTH and transport more ferritin to autophagosomes in the process of IVDD (Figure 4k). Immunofluorescence was used to detect the expression of LC3 and FTH in AFCs and NPCs after TBHP. The picture after fusion showed that some green dots and red dots were in the same position, which indicated that LC3 and FTH were fused, which further proved the existence of ferritinophagy (Figure S2g).

### 3.5 | Silencing of NCOA4 alleviated ferroptosis but did not affect the activity of autophagy

On account of ferritinophagy was involved in TBHP-induced cell death and NCOA4 play an important role in ferritinophagy, we focused on NCOA4-mediated ferritinophagy in AFCs and NPCs. To determine the role of NCOA4 in AFCs and NPCs, AFCs and NPCs were transfected with control siRNA or NCOA4 siRNA to silence the expression of NCOA4. As shown in Figures 5a and 5f, the expression of NCOA4 was knockdown in AFCs and NPCs transfected with NCOA4 siRNA. Transfection of cells was followed by subsequent treatment. As Figures 5a and 5f showed, the silencing of NCOA4 hardly affected the protein level of FTH, GPX4, P62, and LC3II but increased the protein level of FTH and GPX4 caused by TBHP. The upregulation trend of autophagy induced by TBHP was not affected by NCOA4 knockdown in AFCs and NPCs (Figures 5a and 5f). The ratio of ferroptosis marker proteins to β-actin further explained that the silencing of NCOA4 inhibited ferroptosis (Figures 5b,c and 5g,h). The ratio of autophagy marker proteins to β-actin further illustrated that NCOA4 knockdown did not influence the level of autophagy (Figures 5d,e and 5i,j). Using immunofluorescence to detect the expression of GPX4 in AFCs and NPCs treated with control siRNA or NCOA4 siRNA, the results suggested that the fluorescence intensity of GPX4 increased after TBHP treatment in AFCs and NPCs that had been previously silenced NCOA4 compared with the downtrend level of TBHP induced cells previously treated control siRNA (Figures 5k and 5i).

### 3.6 | Overexpression of NCOA4 aggravated the ferroptosis but did not affect the level of autophagy

To confirm whether overexpression of NCOA4 can aggravate the level of ferroptosis in AFCs or NPCs, lenti-NC or lenti-NCOA4 were transfected in AFCs and NPCs before be exposing to TBHP. Western blotting showed that NCOA4 was upregulated in AFCs and NPCs transfected with lenti-NCOA4 compared with Lenti-NC (Figures 6a and 6f). As is shown in the picture, overexpression of NCOA4 hardly affected the protein level of P62 and LC3II but induced the expression of FTH and GPX4 decreased and the protein level of FTH and GPX4 caused by TBHP aggravated (Figures 6a and 6f). The upregulation trend of autophagy induced by TBHP was not affected by NCOA4 overexpression in AFCs and NPCs (Figures 6a and 6f). The ratio of ferroptosis marker proteins to β-actin further demonstrated that overexpression of NCOA4 promoted ferroptosis (Figures 5b,c and 5g,h). The ratio of autophagy marker proteins to β-actin further suggested that NCOA4 knockdown did not influence the level of autophagy (Figures 5d,e and 5i,j). Immunofluorescence results further illustrated that the fluorescence intensity of GPX4 decreased after TBHP treatment in AFCs and NPCs that had been previously overexpressed NCOA4 compared with the level induced by TBHP of cells previously treated lenti-NC (Figures 6k and 6i).

### 3.7 | Inhibiting ferroptosis slowed the process of disc degeneration in vivo

To investigate the relationship between ferroptosis and disc degeneration in vivo, we established the IVDD model using SD rats according to the previous method(D. Xu et al., 2017). Fifteen healthy male adult rats were divided into three groups randomly: control group (a skin incision), saline group, and deferoxamine group. After 8 weeks of model operation, the rats were performed the MRI examination, the results illustrated that the IVD in the model group had degenerated and the degree of disc degeneration is weakened in deferoxamine group compared to the saline group (Figure 7a). The quantification of histological further illustrated that the degree of disc degeneration in the deferoxamine group was less than the saline group (Figure S2h,i). S-O staining and HE staining also showed that the structure of IVD degenerated in the saline group and deferoxamine group and the degree of disc degeneration in the deferoxamine group was lighter than that in the saline group (Figure 7b). Immunohistochemistry showed that the expression of GPX4 and FTH decreased in the saline group compared with the control group and the two proteins level was increased in the deferoxamine group in the contrast of the saline group (Figure 7c,d). Through quantitative analysis of immunohistochemical results, we can also find that the expression of GPX4 and FTH in the saline group was the lowest among the three groups (Figure 7e,f).

## 4 | DISCUSSION

In this study, we illustrate the potential involvement of ferroptosis, induced by oxidative stress and associated with NCOA4-mediated ferritinophagy, in IVDD pathogenesis. Comparison of normal IVD tissue and degenerated IVD tissue, the ferroptosis's marker proteins

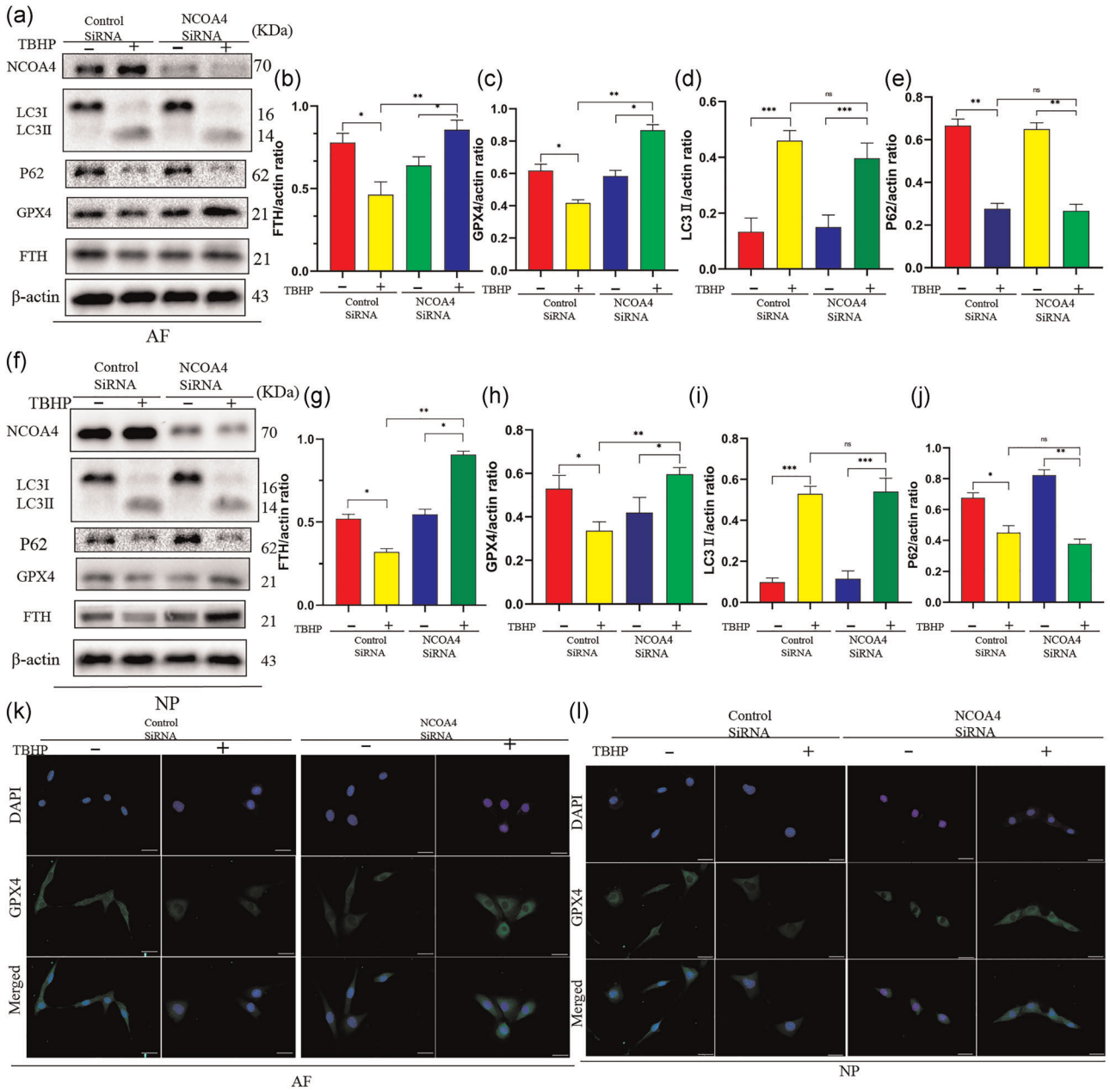


**FIGURE 5** Silencing of nuclear receptor coactivator 4 (NCOA4) inhibited ferroptosis induced by *tert*-butyl hydroperoxide (TBHP) in annulus fibrosus cells (AFCs) and nucleus pulposus cells (NPCs). AFCs and NPCs infected control small interfering RNA (siRNA) or NCOA4 siRNA were exposed to 100 μM TBHP for 3 h. (a) Protein expression of NCOA4, LC3, P62, glutathione peroxidase 4 (GPX4), ferritin heavy chain (FTH), β-actin of AFCs treated TBHP. (b–e) The ratio of protein (FTH, GPX4, LC3II, P62) of β-actin in AFCs. (f) Protein expression of NCOA4, LC3, P62, GPX4, FTH, β-actin of NPCs treated TBHP. (g–j) The ratio of protein (FTH, GPX4, LC3II, P62) of β-actin in NPCs. (k,l) Immunofluorescence detection of protein expression of GPX4 in AFCs and NPCs. ***$p < .001$, **$p < .01$, *$p < .05$ ($n = 3$)

GPX4, FTH expression level significantly declined and PTGS2, ACSL4 increased. Our experiments in AFCs and NPCs using Fer-1, DFO, and RSL3 demonstrate the participation of ferroptosis in TBHP-induced cell death. Interestingly, we found that autophagy-related proteins changed and monitored enhanced autophagic flux when cells exposed to TBHP. To investigate the relationship between autophagy and ferroptosis that happened in AFCs and NPCs, treatment with 3-MA, the antagonist of autophagy, in IVD cells confirmed that ferroptosis induced by TBHP happened in an autophagy-dependent manner. NCOA4 is a selective cargo receptor that can transfer ferritin to the autophagosomes and initiate ferritinophagy which mediated the release of free iron linked to lipid peroxidative during oxidative stress (Kang, Kroemer, & Tang, 2019). NCOA4 knockdown attenuated lipid peroxidation and ferroptosis in response to TBHP stimulation in AFCs and NPCs. However, overexpressing NCOA4 results in the opposite. It further explained a connection between ferritinophagy and TBHP induced AFCs and NPCs ferroptosis. Then we did a Co-IP test and found that increased ferritin bound by

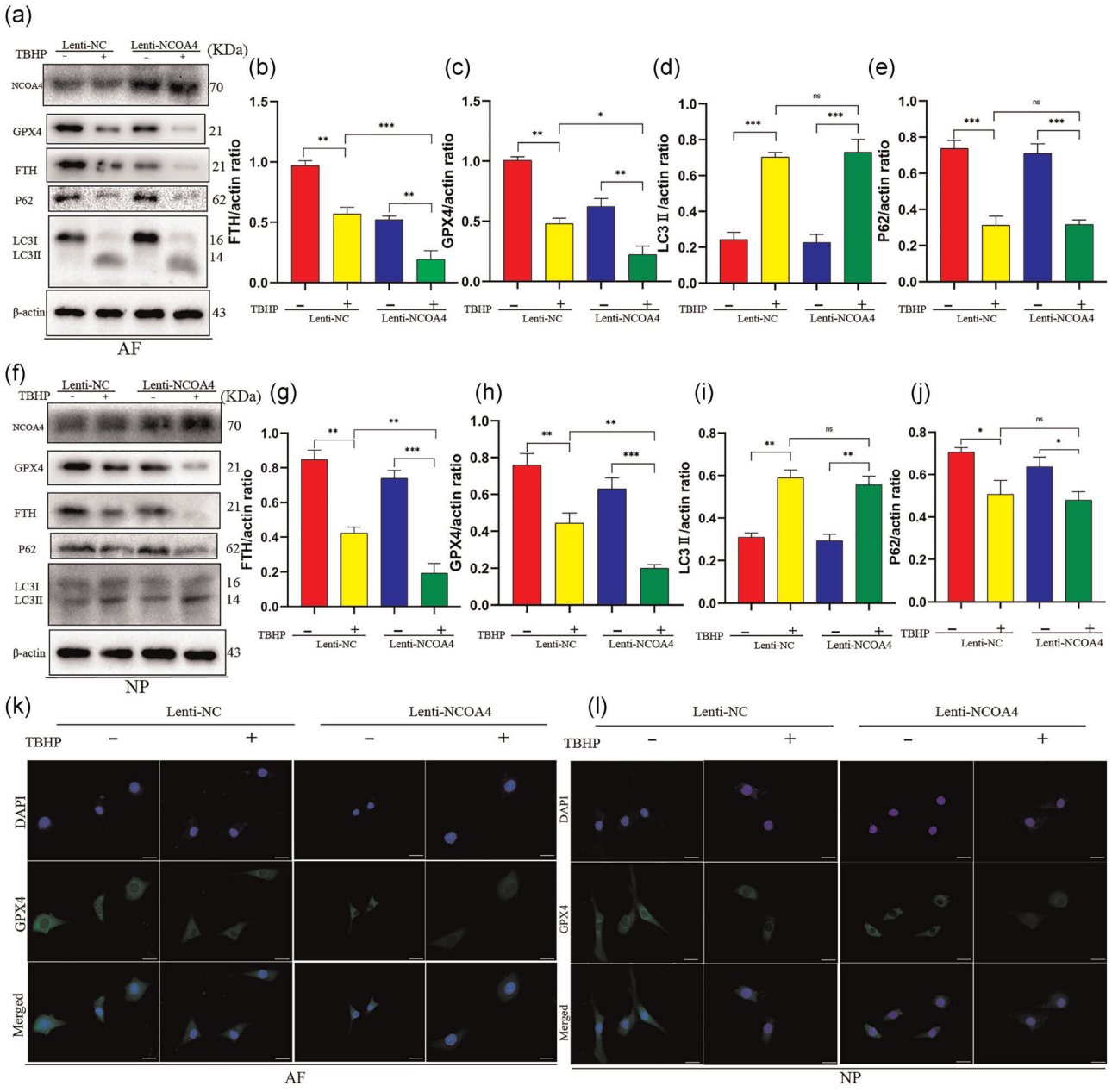


**FIGURE 6** Overexpression of nuclear receptor coactivator 4 (NCOA4) promoted ferroptosis induced by *tert*-butyl hydroperoxide (TBHP) in annulus fibrosus cells (AFCs) and nucleus pulposus cells (NPCs). AFCs and NPCs transfected lenti-NC or lenti-NCOA4 were exposed to 100 μM TBHP for 3 h. (a) Protein expression of NCOA4, LC3, P62, glutathione peroxidase 4 (GPX4), ferritin heavy chain (FTH), β-actin of AFCs. (b–e) The ratio of protein (FTH, GPX4, LC3II, P62) of β-actin in AFCs. (f) Protein expression of NCOA4, LC3, P62, GPX4, FTH, β-actin of NPCs. (g–j) The ratio of protein (FTH, GPX4, LC3II, P62) of β-actin in NPCs. (k,l) Immunofluorescence detection of protein expression of GPX4 in AFCs and NPCs. ***$p < .001$, **$p < .01$, *$p < .05$ ($n = 3$)

NCOA4 when the TBHP-stimulated group compared with the normal group. It further confirmed that NCOA4 transports more ferritin to autophagosomes when oxidative stress occurs in IVD cells and subsequently generate more free iron to cause ferroptosis. From the perspective of animal models, the degree of surgical segment IVDD in the deferoxamine group is reduced in contrast to the saline group. This illustrated ferroptosis involved in the pathogenesis of IVDD in vivo models.

RCD, including necroptosis and apoptosis, in IVD cells, has been illustrated to play a crucial role in IVDD pathogenesis. Apoptosis occurred in NPCs was demonstrated in degenerative discs is connected with tissue degeneration and inflammation (Cheng et al., 2018). Necroptosis involved in APCs and NPCs and enhanced the expression levels of its marker protein RIP3 were illustrated in degenerative disc tissue (Cai et al., 2018). As one of the research hotspots in recent years, ferroptosis, a morphologically different

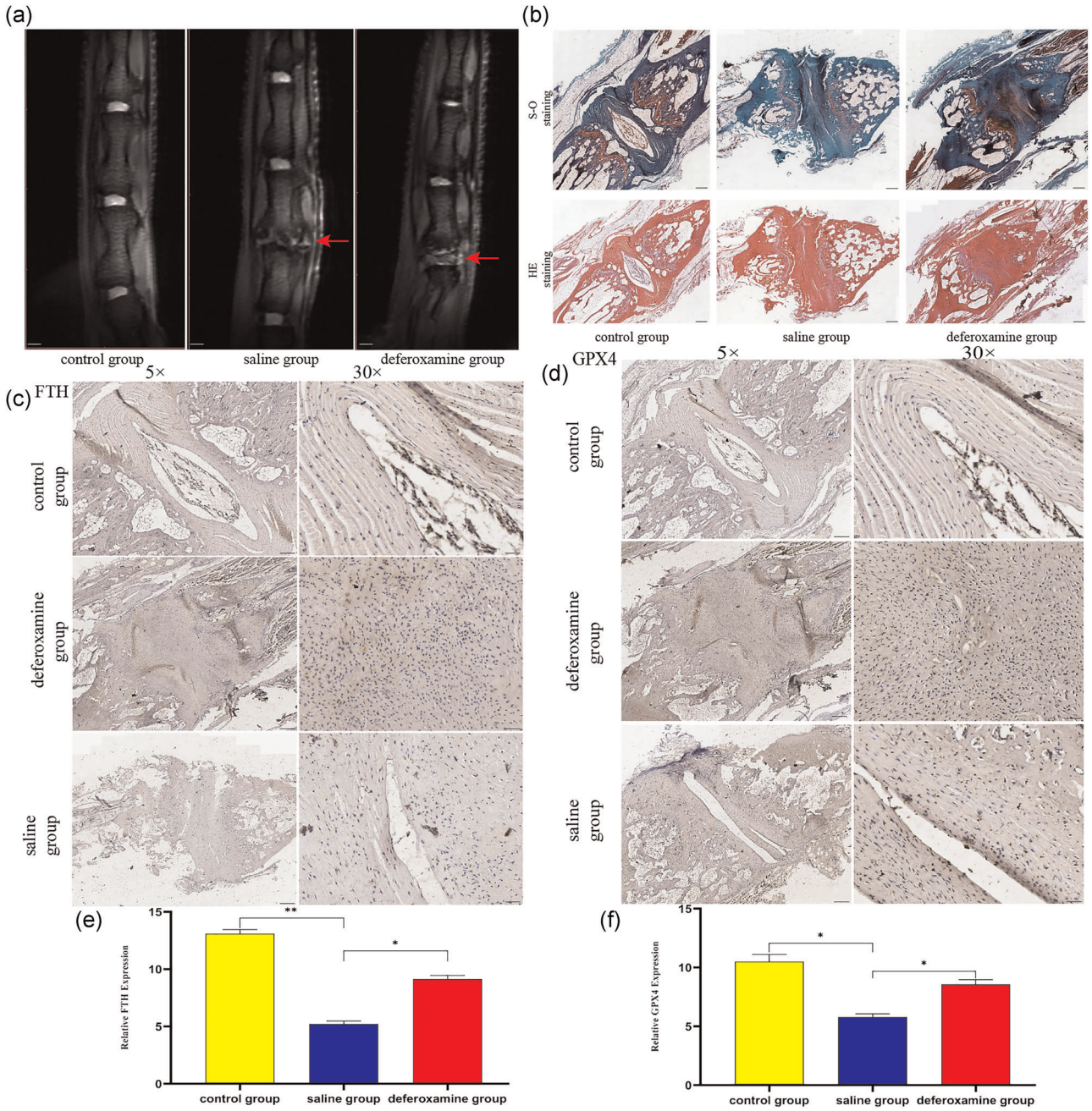


**FIGURE 7** Ferroptosis occurred during the process of intervertebral disc degeneration (IVDD) and suppressing ferroptosis reduced the degree of disc degeneration. (a) T2-weighted magnetic resonance imaging of IVDD models from each group at 8 weeks after molding. (b) Representative safranin O-fast green staining and hematoxylin-eosin staining of disc samples. (c,d) Immunohistochemical staining for ferritin heavy chain (FTH) and glutathione peroxidase 4 (GPX4) expression in the disc samples. (e,f) The expression of FTH and GPX4 in these three groups. $^{**}p < .01$, $^{*}p < .05$ ($n = 3$)

from other forms of RCD, has been intensely reported in both degenerative disease and cancer (Conrad & Pratt, 2019). However, this emerging RCD has not been studied in IVDD. Our in vitro and in vivo experiments have shown that ferroptosis is involved in the pathogenesis of IVDD (Figure 8).

Autophagy, a catabolic process, can maintain cell viability and homeostasis by degrading intracellular substrates in lysosomes in response to hypoxia, oxidative stress, and nutrient stress (Jiang, Overholtzer, & Thompson, 2015). Autophagy participates in IVDD pathogenesis have been reported in terms of inflammatory stimulation and apoptosis (J. Wang et al., 2019; Yi et al., 2019). In recent years, ferritinophagy is considered to be a novel selective autophagic degradation of ferritin, which is mediated by the specific adaptor protein NCOA4 (Mancias et al., 2015, 2014). In vivo experiments, we found that the expression of FTH decreased and NCOA4 increased. Lenti-NCOA4 mediated overexpression and siNCOA4-mediated

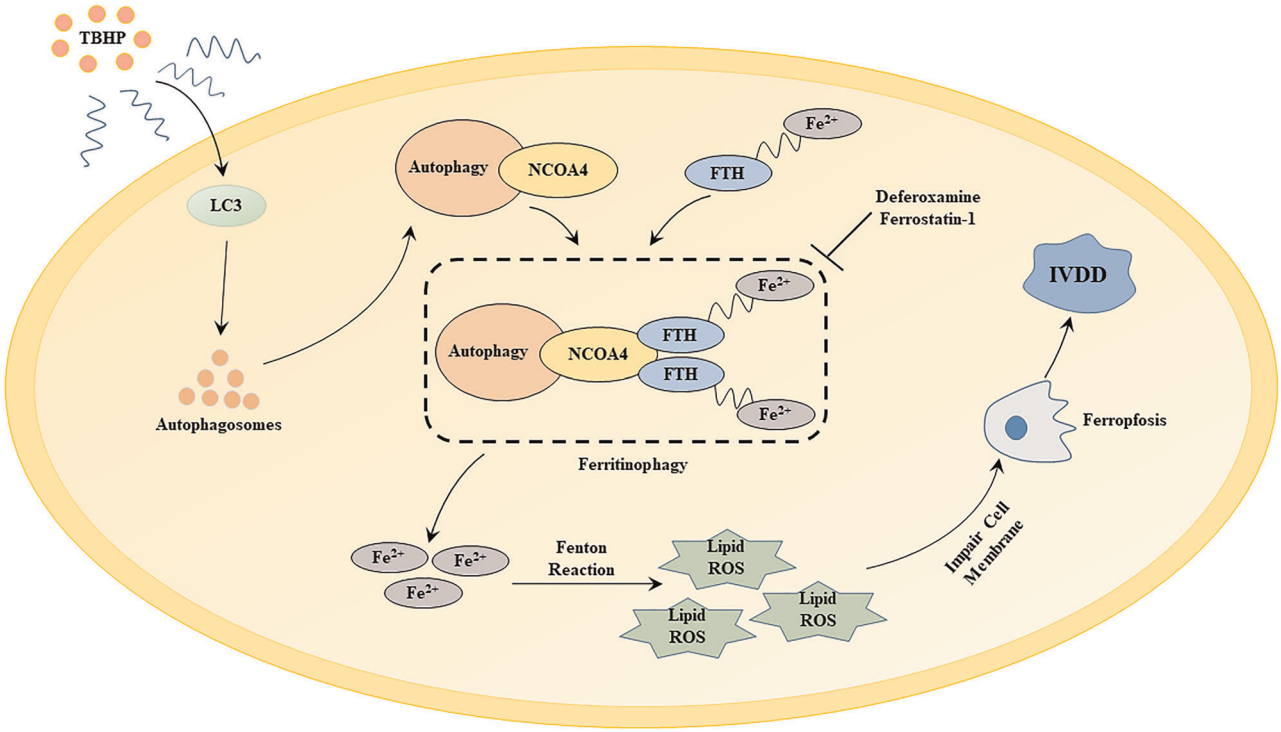


**FIGURE 8** The underlying mechanism of *tert*-butyl hydroperoxide (TBHP)-induced annulus fibrosus cells and nucleus pulposus cells ferroptosis in the process of intervertebral disc degeneration (IVDD). FTH, ferritin heavy chain; NCOA4, nuclear receptor coactivator 4; ROS, reactive oxygen species

knockdown experiments elucidated the role of NCOA4 in ferritin degradation, and CO-IP test further illustrated ferritin and NCOA4 mutually combined, explaining the special role of NCOA4 mediated ferritinophagy in the degradation of ferritin during TBHP stimulation.

In summary, our results support the possible role of ferritinophagy-mediated ferritin degradation and subsequently lipid peroxidation in the pathogenesis of IVDD. Enhancement level of autophagy and increased NCOA4-regulated ferritinophagy when TBHP exposure perhaps at least partly clarifies the destruction of iron homeostasis in degenerative disc tissue. We believe that our findings provide important clues for the development of new IVDD treatment methods by inhibiting ferroptosis.

## ACKNOWLEDGMENT

This study was supported by National Natural Science Foundation of China (Grant No.: 81672206).

## CONFLICT OF INTERESTS

The authors declare that there are no conflict of interest.

## AUTHOR CONTRIBUTIONS

Sheng-Dan Jiang and Lei-Sheng Jiang designed the study. Run-Ze Yang, Wen-Ning Xu, Huo-Liang Zheng, Xin-Feng Zheng, and Bo Li collated the data, carried out data analyses, and produced the initial draft of the manuscript. Sheng-Dan Jiang and Lei-Sheng Jiang contributed to drafting the manuscript. All authors haveread and approved the final submitted manuscript.

## ORCID

*Sheng-Dan Jiang* https://orcid.org/0000-0001-6653-1881

## REFERENCES

Angeli, J. P. F., Shah, R., Pratt, D. A., & Conrad, M. (2017). Ferroptosis inhibition: Mechanisms and opportunities. *Trends in Pharmacological Sciences*, *38*(5), 489–498. https://doi.org/10.1016/j.tips.2017.02.005

Cai, X., Liu, Y., Hu, Y., Liu, X., Jiang, H., Yang, S., & Xiong, L. (2018). ROS-mediated lysosomal membrane permeabilization is involved in bupivacaine-induced death of rabbit intervertebral disc cells. *Redox Biology*, *18*, 65–76. https://doi.org/10.1016/j.redox.2018.06.010

Cao, Z. X., Yang, Y. T., Yu, S., Li, Y. Z., Wang, W. W., Huang, J., & Peng, C. (2017). Pogostone induces autophagy and apoptosis involving PI3K/Akt/mTOR axis in human colorectal carcinoma HCT116 cells. *Journal of Ethnopharmacology*, *202*, 20–27. https://doi.org/10.1016/j.jep.2016.07.028

Cao, C., Zou, J., Liu, X., Shapiro, A., Moral, M., Luo, Z., & Ebraheim, N. (2015). Bone marrow mesenchymal stem cells slow intervertebral disc degeneration through the NF-kappa B pathway. *The Spine Journal*, *15*(3), 530–538. https://doi.org/10.1016/j.spinee.2014.11.021

Cheng, X., Zhang, L., Zhang, K., Zhang, G., Hu, Y., Sun, X., & Zhao, J. (2018). Circular RNA VMA21 protects against intervertebral disc degeneration through targeting miR-200c and X linked inhibitor-of-apoptosis protein. *Annals of the Rheumatic Diseases*, *77*(5), 770–779. https://doi.org/10.1136/annrheumdis-2017-212056

Conrad, M., & Pratt, D. A. (2019). The chemical basis of ferroptosis. *Nature Chemical Biology*, *15*(12), 1137–1147. https://doi.org/10.1038/s41589-019-0408-1

Dimozi, A., Mavrogonatou, E., Sklirou, A., & Kletsas, D. (2015). Oxidative stress inhibits the proliferation, induces premature senescence and promotes a catabolic phenotype in human nucleus pulposus intervertebral disc cells. *European Cells & Materials*, *30*, 89–102. https://doi.org/10.22203/ecm.v030a07

Dixon, S. J., Lemberg, K. M., Lamprecht, M. R., Skouta, R., Zaitsev, E. M., Gleason, C. E., & Stockwell, B. R. (2012). Ferroptosis: An iron-dependent form of nonapoptotic cell death. *Cell*, *149*(5), 1060–1072. https://doi.org/10.1016/j.cell.2012.03.042

Dowdle, W. E., Nyfeler, B., Nagel, J., Elling, R. A., Liu, S., Triantafellow, E., & Murphy, L. O. (2014). Selective VPS34 inhibitor blocks autophagy and uncovers a role for NCOA4 in ferritin degradation and iron homeostasis in vivo. *Nature Cell Biology*, *16*(11), 1069–1079. https://doi.org/10.1038/ncb3053

Feng, C., Liu, H., Yang, M., Zhang, Y., Huang, B., & Zhou, Y. (2016). Disc cell senescence in intervertebral disc degeneration: Causes and molecular pathways. *Cell Cycle*, *15*(13), 1674–1684. https://doi.org/10.1080/15384101.2016.1152433

Friedmann Angeli, J. P., Schneider, M., Proneth, B., Tyurina, Y. Y., Tyurin, V. A., Hammond, V. J., & Conrad, M. (2014). Inactivation of the ferroptosis regulator Gpx4 triggers acute renal failure in mice. *Nature Cell Biology*, *16*(12), 1180–1191. https://doi.org/10.1038/ncb3064

Fujii, S., Hara, H., Araya, J., Takasaka, N., Kojima, J., Ito, S., & Kuwano, K. (2012). Insufficient autophagy promotes bronchial epithelial cell senescence in chronic obstructive pulmonary disease. *Oncoimmunology*, *1*(5), 630–641. https://doi.org/10.4161/onci.20297

Gao, M., Monian, P., Pan, Q., Zhang, W., Xiang, J., & Jiang, X. (2016). Ferroptosis is an autophagic cell death process. *Cell Research*, *26*(9), 1021–1032. https://doi.org/10.1038/cr.2016.95

Gao, M., Monian, P., Quadri, N., Ramasamy, R., & Jiang, X. (2015). Glutaminolysis and transferrin regulate ferroptosis. *Molecular Cell*, *59*(2), 298–308. https://doi.org/10.1016/j.molcel.2015.06.011

Han, B., Zhu, K., Li, F. C., Xiao, Y. X., Feng, J., Shi, Z. L., & Chen, Q. X. (2008). A simple disc degeneration model induced by percutaneous needle puncture in the rat tail. *Spine*, *33*(18), 1925–1934. https://doi.org/10.1097/BRS.0b013e31817c64a9

Henry, N., Clouet, J., Le Bideau, J., Le Visage, C., & Guicheux, J. (2018). Innovative strategies for intervertebral disc regenerative medicine: From cell therapies to multiscale delivery systems. *Biotechnology Advances*, *36*(1), 281–294. https://doi.org/10.1016/j.biotechadv.2017.11.009

Hou, W., Xie, Y., Song, X., Sun, X., Lotze, M. T., Zeh, H. J., 3rd, & Tang, D. (2016). Autophagy promotes ferroptosis by degradation of ferritin. *Autophagy*, *12*(8), 1425–1428. https://doi.org/10.1080/15548627.2016.1187366

Imai, H., Hirao, F., Sakamoto, T., Sekine, K., Mizukura, Y., Saito, M., & Nakagawa, Y. (2003). Early embryonic lethality caused by targeted disruption of the mouse PHGPx gene. *Biochemical and Biophysical Research Communications*, *305*(2), 278–286. https://doi.org/10.1016/s0006-291x(03)00734-4

Ito, S., Araya, J., Kurita, Y., Kobayashi, K., Takasaka, N., Yoshida, M., & Kuwano, K. (2015). PARK2-mediated mitophagy is involved in regulation of HBEC senescence in COPD pathogenesis. *Autophagy*, *11*(3), 547–559. https://doi.org/10.1080/15548627.2015.1017190

Jensen, C. E., Riis, A., Petersen, K. D., Jensen, M. B., & Pedersen, K. M. (2017). Economic evaluation of an implementation strategy for the management of low back pain in general practice. *Pain*, *158*(5), 891–899. https://doi.org/10.1097/j.pain.0000000000000851

Jeong, S. W., Lee, J. S., & Kim, K. W. (2014). In vitro lifespan and senescence mechanisms of human nucleus pulposus chondrocytes. *The Spine Journal*, *14*(3), 499–504. https://doi.org/10.1016/j.spinee.2013.06.099

Jiang, X., Overholtzer, M., & Thompson, C. B. (2015). Autophagy in cellular metabolism and cancer. *Journal of Clinical Investigation*, *125*(1), 47–54. https://doi.org/10.1172/jci73942

Kang, R., Kroemer, G., & Tang, D. (2019). The tumor suppressor protein p53 and the ferroptosis network. *Free Radical Biology and Medicine*, *133*, 162–168. https://doi.org/10.1016/j.freeradbiomed.2018.05.074

Lee, Y. S., Kalimuthu, K., Seok Park, Y., Makala, H., Watkins, S. C., Choudry, M. H. A., & Lee, Y. J. (2020). Ferroptotic agent-induced endoplasmic reticulum stress response plays a pivotal role in the autophagic process outcome. *Journal of Cellular Physiology*, *235*, 6767–6778. https://doi.org/10.1002/jcp.29571

Li, Q., Han, X., Lan, X., Gao, Y., Wan, J., Durham, F., & Wang, J. (2017). Inhibition of neuronal ferroptosis protects hemorrhagic brain. *JCI Insight*, *2*(7), e90777. https://doi.org/10.1172/jci.insight.90777

Linkermann, A., Stockwell, B. R., Krautwald, S., & Anders, H. J. (2014). Regulated cell death and inflammation: An auto-amplification loop causes organ failure. *Nature Reviews Immunology*, *14*(11), 759–767. https://doi.org/10.1038/nri3743

Le Maitre, C. L., Binch, A. L., Thorpe, A. A., & Hughes, S. P. (2015). Degeneration of the intervertebral disc with new approaches for treating low back pain. *Journal of Neurosurgical Sciences*, *59*(1), 47–61.

Mancias, J. D., Pontano Vaites, L., Nissim, S., Biancur, D. E., Kim, A. J., Wang, X., & Harper, J. W. (2015). Ferritinophagy via NCOA4 is required for erythropoiesis and is regulated by iron dependent HERC2-mediated proteolysis. *eLife*, *4*, e10308. https://doi.org/10.7554/eLife.10308

Mancias, J. D., Wang, X., Gygi, S. P., Harper, J. W., & Kimmelman, A. C. (2014). Quantitative proteomics identifies NCOA4 as the cargo receptor mediating ferritinophagy. *Nature*, *509*(7498), 105–109. https://doi.org/10.1038/nature13148

Martin-Sanchez, D., Ruiz-Andres, O., Poveda, J., Carrasco, S., Cannata-Ortiz, P., Sanchez-Nino, M. D., & Sanz, A. B. (2017). Ferroptosis, but not necroptosis, is important in nephrotoxic folic acid-induced AKI. *Journal of the American Society of Nephrology*, *28*(1), 218–229. https://doi.org/10.1681/asn.2015121376

Nasto, L. A., Robinson, A. R., Ngo, K., Clauson, C. L., Dong, Q., St. Croix, C., & Vo, N. V. (2013). Mitochondrial-derived reactive oxygen species (ROS) play a causal role in aging-related intervertebral disc degeneration. *Journal of Orthopaedic Research*, *31*(7), 1150–1157. https://doi.org/10.1002/jor.22320

Nerlich, A. G., Bachmeier, B. E., Schleicher, E., Rohrbach, H., Paesold, G., & Boos, N. (2007). Immunomorphological analysis of RAGE receptor expression and NF-kappa B activation in tissue samples from normal and degenerated intervertebral discs of various ages. *Annals of the New York Academy of Sciences*, *1096*, 239–248. https://doi.org/10.1196/annals.1397.090

Pasparakis, M., & Vandenabeele, P. (2015). Necroptosis and its role in inflammation. *Nature*, *517*(7534), 311–320. https://doi.org/10.1038/nature14191

Shamji, M. F., Setton, L. A., Jarvis, W., So, S., Chen, J., Jing, L., & Richardson, W. J. (2010). Proinflammatory cytokine expression profile in degenerated and herniated human intervertebral disc tissues. *Arthtitis and Rheumatism*, *62*(7), 1974–1982. https://doi.org/10.1002/art.27444

Stockwell, B. R., Friedmann Angeli, J. P., Bayir, H., Bush, A. I., Conrad, M., Dixon, S. J., & Zhang, D. D. (2017). Ferroptosis: A regulated cell death nexus linking metabolism, redox biology, and disease. *Cell*, *171*(2), 273–285. https://doi.org/10.1016/j.cell.2017.09.021

Vo, N., Niedernhofer, L. J., Nasto, L. A., Jacobs, L., Robbins, P. D., Kang, J., & Evans, C. H. (2013). An overview of underlying causes and animal models for the study of age-related degenerative disorders of the

spine and synovial joints. *Journal of Orthopaedic Research*, *31*(6), 831–837. https://doi.org/10.1002/jor.22204

Wang, J., Hu, J., Chen, X., Huang, C., Lin, J., Shao, Z., & Zhang, X. (2019). BRD4 inhibition regulates MAPK, NF-κB signals, and autophagy to suppress MMP-13 expression in diabetic intervertebral disc degeneration. *FASEB Journal*, *33*(10), 11555–11566. https://doi.org/10.1096/fj.201900703R

Wang, X., Wang, H., Yang, H., Li, J., Cai, Q., Shapiro, I. M., & Risbud, M. V. (2014). Tumor necrosis factor-α- and interleukin-1β-dependent matrix metalloproteinase-3 expression in nucleus pulposus cells requires cooperative signaling via syndecan 4 and mitogen-activated protein kinase-NF-kappa B axis: Implications in inflammatory disc disease. *American Journal of Pathology*, *184*(9), 2560–2572. https://doi.org/10.1016/j.ajpath.2014.06.006

Wang, Q., Zhu, J., Zhang, K., Jiang, C., Wang, Y., Yuan, Y., & Liu, Z. (2013). Induction of cytoprotective autophagy in PC-12 cells by cadmium. *Biochemical and Biophysical Research Communications*, *438*(1), 186–192. https://doi.org/10.1016/j.bbrc.2013.07.050

World Medical Association. (2014). World Medical Association Declaration of Helsinki: ethical principles for medical research involving human subjects. *Journal of the American College of Dentists*, *81*(3), 14–18.

Xie, Y., Hou, W., Song, X., Yu, Y., Huang, J., Sun, X., & Tang, D. (2016). Ferroptosis: Process and function. *Cell Death and Differentiation*, *23*(3), 369–379. https://doi.org/10.1038/cdd.2015.158

Xu, D., Jin, H., Wen, J., Chen, J., Chen, D., Cai, N., & Wang, X. (2017). Hydrogen sulfide protects against endoplasmic reticulum stress and mitochondrial injury in nucleus pulposus cells and ameliorates intervertebral disc degeneration. *Pharmacological Research*, *117*, 357–369. https://doi.org/10.1016/j.phrs.2017.01.005

Xu, W. N., Yang, R. Z., Zheng, H. L., Yu, W., Zheng, X. F., Li, B., & Jiang, L. S. (2019). PGC-1α acts as an mediator of Sirtuin2 to protect annulus fibrosus from apoptosis induced by oxidative stress through restraining mitophagy. *International Journal of Biological Macromolecules*, *136*, 1007–1017. https://doi.org/10.1016/j.ijbiomac.2019.06.163

Yang, H., Cao, C., Wu, C., Yuan, C., Gu, Q., Shi, Q., & Zou, J. (2015). TGF-βl suppresses inflammation in cell therapy for intervertebral disc degeneration. *Scientific Reports*, *5*, 13254. https://doi.org/10.1038/srep13254

Yang, H., Yuan, C., Wu, C., Qian, J., Shi, Q., Li, X., & Zou, J. (2016). The role of TGF-β1/Smad2/3 pathway in platelet-rich plasma in retarding intervertebral disc degeneration. *Journal of Cellular and Molecular Medicine*, *20*(8), 1542–1549. https://doi.org/10.1111/jcmm.12847

Yi, W., Wen, Y., Tan, F., Liu, X., Lan, H., Ye, H., & Liu, B. (2019). Impact of NF-κB pathway on the apoptosis-inflammation-autophagy crosstalk in human degenerative nucleus pulposus cells. *Aging*, *11*(17), 7294–7306. https://doi.org/10.18632/aging.102266

## SUPPORTING INFORMATION

Additional Supporting Information may be found online in the supporting information tab for this article.

**How to cite this article:** Yang R-Z, Xu W-N, Zheng H-L, et al. Involvement of oxidative stress-induced annulus fibrosus cell and nucleus pulposus cell ferroptosis in intervertebral disc degeneration pathogenesis. *J Cell Physiol*. 2021;236: 2725–2739. https://doi.org/10.1002/jcp.30039